BUILD SIMUL (2014) 7: 35 – 55
DOI 10.1007/s12273-013-0103-1

Detailing the effects of geometry approximation and grid simplification on the capability of a CFD model to address the benchmark test case for flow around a computer simulated person

Giacomo Villi (✉), Michele De Carli

Department of Industrial Engineering, Università degli Studi di Padova, Padua, Italy

Abstract

This paper details the use of a simplified CFD model to predict the flow patterns around a computer simulated person in a displacement ventilated room. The use of CFD is a valuable tool for indoor airflow analysis and the level of complexity of the model being investigated is often critical to the accuracy of predictions. The closer the computational geometry is to the real geometry of interest, the more accurate the corresponding results are expected to be. High complexity meshes enable elaborated geometries to be resolved. The drawback is, however, their increased computational cost. The Fire Dynamics Simulator (FDS) model (Version 5) enabled to investigate the effects of geometry and computational grid simplification on the accuracy of numerical predictions. The FDS model is based on a three-dimensional Cartesian coordinate system and all solid obstructions are forced to conform to the underlying numerical grid which is a potential limitation when dealing with complex geometries such as those of a human body. Nevertheless, the developed computational model was based exclusively on a three-dimensional rectangular geometry. At the same time, in order to limit the total number of grid cells, a relatively coarser grid than those used for similar simulations was adopted in the investigation. The developed model was then assessed in terms of its capability of reproducing benchmark temperature and air velocity distributions. The extent to which numerical results depend on different simulation settings was detailed and different boundary conditions are discussed in order to provide some guidance on the parameters that resulted to affect the accuracy of the predicted results. The comparison between numerical results and measurements showed that a simplified CFD model can be used to capture the airflow characteristics of the investigated scenario with predictions showing a favourable agreement with experimental data at least in the qualitative features of the flow (the detailed investigation of the local airflow field near the occupant can not be probably conducted apart from considering the real human geometry). Significant influence of simulator geometry and of boundary conditions was found.

Keywords

LES,
indoor airflow,
CFD,
ventilation

Article History

Received: 17 July 2012
Revised: 29 November 2012
Accepted: 18 December 2012

© Tsinghua University Press and Springer-Verlag Berlin Heidelberg 2013

1 Introduction

Air distribution in rooms is the result of the complex interaction between the ventilation system and local disturbances induced by factors such as occupants. A more detailed investigation of the distribution of air properties such as temperature and velocity within a room is beneficial to the design of an energy efficient, comfortable and healthy indoor environment. In order to predict the details of the ventilation mechanism, realistic conditions such as the presence of obstructions and localized heat sources have to be incorporated into the analysis. A person acts as an obstacle when exposed to a flow (Brohus 1997); behind the person a wake is generated whilst in front some air is pushed away. The human body is continually exchanging energy with the surrounding environment and the excess human temperature results in an ascending plume with velocities which can exceed 0.2 m/s and even reach 0.5 m/s locally (Zukowska et al. 2007). A nude

E-mail: giacomo.villi@unipd.it

standing subject at 20℃ room temperature can result in up to 60 L/s of passing air over the head at a maximum velocity of 0.25 m/s, extending up to 2 m above the head (Bolashikov 2010). The convection plume rising from the human body acts as an active contributor to the mixing in a room: the mixing time (i.e. the time from the instantaneous release of a point source pollutant until the relative standard deviation of concentrations drops permanently below 10%) associated to a standing body in a 31 m^3 room is about 45 minutes (Mora and Gadgil 2002). The understanding of such interactions is important to room ventilation design and air pollution control (Craven and Settles 2006).

Two approaches are available for the investigation of indoor airflows: experimental measurement and computer simulation (Liu et al. 2012). Full scale experiments provide the most reliable data but obtaining accurate indoor airflow measurements is expensive and may take long to be completed. Computational fluid dynamics (CFD) is alternative to full scale measurements. CFD is less expensive and can obtain data much faster due to the continuous development in computing power and in numerical routines. Moreover, CFD provides details on the entire flow field which is not possible with experimental methods. However, there are some disadvantages of CFD when compared to other methods of investigation and, in particular, the computing speed persists as a main drawback. In order to broaden the applicability of CFD methods to indoor airflow simulation, efforts have been put on developing simplified turbulence models and on testing coarser than "standard" grid systems (Zhai and Wang 2011).

The decision to use a CFD model requires that the accuracy of predictions and the error scales which are brought have to be evaluated. The numerical simulation of airflow around a person using CFD is challenging because of the details of the human body geometry and the corresponding complicated airflow patterns generated. Moreover, the accurate prediction of features such as the buoyancy driven flow from the human body often requires that the computational grid is adapted such that its density is greatest near the model where proper resolution of the boundary layer is desired (Craven and Settles 2006). Different levels of complexity are used in CFD models to predict local airflow and personal microenvironment. Simplified CFD models can provide reduced computing time, less effort needed in grid generation and faster results but the circumstances under which they adversely affect simulation accuracy have to be carefully evaluated.

The Fire Dynamics Simulator (FDS) is a Fortran based, three-dimensional model developed by the U.S. National Institute of Standards and Technology (NIST); turbulence is modelled using the large eddy simulation (LES) approach. Although originally developed for fire related scenarios, the model has already been successfully applied to indoor airflow analysis. The FDS capability of reproducing the flow characteristics of a displacement ventilated occupied room is presently discussed.

The structure of the paper is as follows. An overview on the CFD approach to fluid flow modelling is presented. Then, the paper briefly describes the FDS model and, finally, the FDS application to the simulation of the flow around the room occupant is detailed by comparing numerical results to experimental data.

The objective of this paper is twofold. Firstly, the validation work aims at providing deeper knowledge on the capability of a simplified computational approach of capturing the features of complex room airflows such those in which persons are involved. FDS requires that a complex geometry, such as the human body, has to be simplified to fit a Cartesian grid. The paper presents different geometries of a standing person and then illustrates, by providing quantitative information about the global error, to what extent a rectangular geometry is able to reproduce the flow characteristics of the investigated test case. In general, the computational domain may consist of one or more rectangular meshes, each with its own user defined three-dimensional rectilinear grid system. Although multi-mesh models with different grid sizes are allowed for and meshes can abut or overlap, features such as the modification of an existing mesh (i.e. mesh adaptation) or the creation of prism layers are not implemented in the model. The performed investigation aims at determining the effects on simulation accuracy and on the required computing times found by allowing coarser grids than those documented in previous studies about the analyzed test case.

Secondly, the comparison between simulation results and experimental data enabled to identify a number of possible sources of uncertainty which have been further investigated in detail. Boundary conditions and physical models represent the means through which the user controls the fluxes (mass, momentum and energy) entering and leaving the computational domain and the corresponding physical behaviour and, therefore, they are of key importance for the accuracy of CFD predictions. The appropriateness of physical models and boundary conditions has been discussed in order to provide some guidance on the parameters that had an impact on results accuracy.

The results of the presented verification are meant to evaluate the capability of a simplified CFD approach of addressing thermal comfort issues and personal exposure to contaminants (such as in (Shih and Lee 2004)). Moreover, specifically as to the FDS use, the investigation of the capability of reproducing the interaction between a person and the general flow field has implications on the modelling of the initial stages of fires which are dominated by ordinary indoor airflow phenomena (Musser et al. 2001).

1.1 CFD theory and literature review

CFD consists of the application of numerical techniques to solve the Navier-Stokes equations which describe fluid flow. Most of room airflows are non isothermal, three-dimensional and turbulent where turbulence modelling represents the key distinguishing feature of any CFD model.

Direct numerical simulation (DNS) can resolve the flow field up to the smallest length scale. However, DNS is not viable for indoor analysis because of the number of the required grid cells (quantifiable in the order of $Re^{9/4}$ (Zhai et al. 2007)) which is prohibitive even for modern computers.

The Reynolds Averaged Navier-Stokes (RANS) equations solve the statistically time averaged Navier-Stokes equations. Decomposing flow quantities into a mean value with a fluctuating component superimposed on it and the process of time averaging introduce new terms so that various turbulence models are used to bring closure to the RANS equations. RANS equations solve mean flow quantities only with all the scales of the turbulence being modelled.

The LES approach is based on the hypothesis that turbulent flow can be separated into large and small scale eddies. Large eddies, which carry the bulk of mass, momentum and energy in a flow are difficult to be parameterized as they are markedly case dependent and so they are instead fully resolved in the computation. Small scale eddies which are produced by the energy cascade process from larger eddies are less sensitive to the details of the specific problem, more isotropic and more universal. Although not being directly captured as they occur on length scales which are smaller than the adopted grid cell size, they are accounted for by appropriate sub-grid models.

Wang et al. (2007) investigated a slot ventilated enclosure by applying both RANS and LES and simulation results were compared to experimental measurements. It resulted that both RANS and LES were able to predict flow characteristics which were observed in the experiments; nevertheless, LES reproduced more accurately some features of the experimental flow structures such as corner vortices. Jiang et al. (2009) used CFD to investigate the airflow within a full scale room and the volumetric particle velocimetry enabled to characterize experimentally the three spatial components of air velocities. It was found that among the different turbulence models investigated, LES resulted in the best predictions for all the conditions considered in the analysis.

Caciolo et al. (2012) contrasted the results of a RANS model and a LES model when applied to single side natural ventilation. Three full scale experiments were performed in a test building and experimental conditions were reproduced numerically by means of CFD. Based on the agreement with experiments, it resulted that LES provided more accurate results than RANS. However, LES required computational costs which were estimated in 30 times higher than those of RANS.

1.2 The FDS model

LES has been traditionally limited by the required computing cost. However, if only regular geometries are allowed, a fast solver can limit the effort as the natural ordering of rectangular blocks can enable the use of efficient numerical algorithms for solving the discretized form of the conservation equations. This approach has led to the development of the Fire Dynamics Simulator where the equations of mass, momentum and energy conservation are solved for on a three-dimensional, rectilinear grid. A modified form of the Navier-Stokes equations appropriate for low-speed thermally-driven flow is implemented in the model; all spatial derivatives in the conservation equations are discretized by second order finite difference scheme and all the thermodynamic variables are updated in time by means of an explicit second order predictor-corrector scheme (McGrattan et al. 2010a). Sub-grid modelling is performed by means of the Smagorinsky model which is based on the eddy viscosity assumption. FDS offers several advantages over other CFD models as fast computational speed and relatively modest requirements in terms of computational resources (Hostikka 2011). The main disadvantages are the restriction to regular geometries and the lack of graphical input capability (Emmerich 1997).

FDS was officially released in 2000. Although it has been predominantly used in fire safety engineering, the low Mach number assumption is also appropriate to describe building ventilation scenarios which do not include fires (McGrattan et al. 2010b).

Emmerich and McGrattan (1998) investigated the application of NIST-LES3D, from which FDS evolved, to analyze a forced convection test case in a three-dimensional ventilated room. It was found that simulation results agreed favourably with experimental data for the main portion of the room. Different examples of how the model can be used to investigate indoor airflow scenarios were presented by Musser et al. (2001). By comparing FDS simulations to six published sets of experimental data of which four involved non fire cases, it was found that results were accurate enough to agree positively with experiments. Lin et al. (2006) presented the comparison between FDS predictions and experimental data with reference to the airflow in a cabin model. It resulted a good correlation between CFD predictions and PIV (particle image velocimetry) measurements. Cho and Liu (2010) used FDS to investigate the correlation between minimum airflow, discharge temperature and room

thermal comfort. Near optimal conditions were identified by means of CFD simulations and the corresponding performance was positively evaluated through field experiments. Farnham et al. (2011) investigated the cooling potential of misting nozzles. Good agreement was found between numerical results and experimental measurements.

1.2.1 Brief review of the key equations in the FDS model

A detailed description of the mathematical model and the governing equations is provided in (McGrattan et al. 2010c; McGrattan et al. 2012; McDermott et al. 2010)

The conservation of mass equation is written as follows:

$$\frac{\partial \rho}{\partial t} + \nabla \cdot (\rho \vec{u}) = \dot{m}_b''' \tag{1}$$

where $\dot{m}_b'''$ represents the addition of mass from subgrid scale particles (e.g. evaporating droplets) and any type of unresolvable object.

Based on the low Mach assumption, pressure, p, is decomposed into a "background" component $\overline{p}(z,t)$ (z stands for the spatial coordinate in the gravity direction) and a perturbation $\tilde{p}(x,y,z,t)$ which drives the fluid motion. As it can be assumed that for low Mach number flows temperature and density are inversely proportional only the background pressure is retained in the equation of state:

$$\overline{p} = \frac{\rho R T}{\overline{W}} \tag{2}$$

where R = 8.3145 kJ/(kmol·K) is the gas law constant.

The energy conservation equation is written in terms of the sensible enthalpy h_s as follows:

$$\frac{\delta}{\delta t}(\rho h_s) + \nabla \cdot (\rho h_s \vec{u}) = \frac{\mathrm{D}p}{\mathrm{D}t} + \dot{q}''' - \dot{q}_b''' - \nabla \cdot \vec{q}'' + \varepsilon \tag{3}$$

where $\dot{q}'''$ takes into account the heat release rate per unit volume from a chemical reaction (e.g. the fire), the term $\dot{q}_b'''$ stands for the energy transferred to subgrid objects (e.g. evaporating droplets) and the term $\vec{q}''$ combines the conductive and radiative heat fluxes. ε stands for the rate at which kinetic energy is transferred to thermal energy due to the viscosity of the fluid. Taking advantage of the low Mach number assumption, Eq. (3) is not solved explicitly being its source terms included in the formulation for the flow divergence which is obtained by combining the mass conservation equation (Eq. (1)) and the material derivative of the equation of state (Eq. (2)):

$$\nabla \cdot \vec{u} = \frac{1}{\rho}\left(\dot{m}_b''' - \frac{\mathrm{D}\rho}{\mathrm{D}t}\right) = \frac{1}{\rho}\dot{m}_b''' - \frac{1}{\overline{p}}\frac{\mathrm{D}\overline{p}}{\mathrm{D}t} + \overline{W}\frac{\mathrm{D}}{\mathrm{D}t}\left(\frac{1}{\overline{W}}\right) + \frac{1}{T}\frac{\mathrm{D}T}{\mathrm{D}t} \tag{4}$$

where the right hand side includes the source and diffusion terms from the mass, species and energy conservation equations.

The momentum equation is given by

$$\frac{\partial \vec{u}}{\partial t} + \vec{F} + \nabla H = 0 \tag{5}$$

where $H = |\vec{u}|^2/2 + \tilde{p}/\rho$ stands for the pressure gradient and the vector $\vec{F}$ is defined as follows:

$$\vec{F} = -\vec{u} \times \vec{\omega} + \left(\frac{1}{\rho} - \frac{1}{\rho_\infty}\right)\nabla \tilde{p} - \frac{1}{\rho}\left((\rho - \rho_0)\vec{g} + \vec{f}_b + \nabla \cdot \tau_{ij}\right) \tag{6}$$

where $\vec{f}_b$ represents the external force vector, τ_{ij} is the viscous stress tensor, $\vec{\omega} = (\omega_x, \omega_y, \omega_z)$ stands for the vorticity vector.

By taking the divergence of the momentum equation (Eq. (5)), a Poisson equation for the pressure is derived:

$$\nabla^2 H = -\frac{\partial}{\partial t}(\nabla \cdot \vec{u}) - \nabla \cdot \vec{F} \tag{7}$$

It results a constant coefficient form of the Poisson equation for which are available direct (i.e. non iterative) solvers optimized for uniform grids. Because FDS was specifically developed for rectilinear grids, it is able to obtain the pressure field with only one pass through the solver.

Near wall modelling is a key issue in CFD simulations. Therefore, it is useful to briefly describe how the velocity gradient at walls is calculated in the FDS model. As it was developed for large scale investigations such as the fire related problems, FDS was written with the intention that relatively coarser grids would have been used with respect to the standard CFD practice (Musser et al. 2001).

The near wall region is characterized by small structures (eddies) which would require much finer mesh compared to the grid in the outer region to be fully resolved. In order to combine a reduction in the resource requirements due to the severe near wall resolution which would enable the near wall region to be fully resolved to a realistic description of the resulting effects on the overall flow field, a wall-layer model can be used to provide an estimate of the instantaneous wall shear stress at the wall nearest node which is then used as a wall boundary condition (Temmerman et al. 2003).

The near wall velocity distribution can be expressed by the following relationship which is called the "law of the wall" (Versteeg and Malalasekera 1995):

$$u^+ = \frac{u}{u_\tau} = f\left(\frac{\rho u_\tau y}{\mu}\right) = f(y^+) \tag{8}$$

where u^+ is the dimensionless velocity, $u_\tau = \sqrt{\tau_w/\rho}$ stands for the so called friction velocity, τ_w is the wall shear stress and ρ is the fluid density.

The Werner and Wengle model proposes the following velocity wall profile:

$$u^+ = \begin{cases} y^+ \text{ if } y^+ \leqslant 11.8 \\ 8.3(y^+)^{1/7} \text{ if } y^+ > 11.8 \end{cases} \quad (9)$$

More details on model implementation may be found in (McDermott 2009).

The convective heat transfer model is based on a combination of natural and forced convection correlations. A forced convection heat transfer coefficient and a natural heat transfer coefficient are calculated based on the following expressions respectively:

$$\frac{k}{L}0.037Re^{4/5}Pr^{1/3} \quad (10)$$

$$C\Delta T^{1/3} \quad (11)$$

where C(W/(m^2·K$^{4/3}$)) is the coefficient for natural convection (by default, 1.52 for a horizontal surface and 1.31 for a vertical surface). The greater of the two is used to calculate the convective heat transfer.

The FDS model includes radiative heat transfer via the solution of the radiation transport equation for a non scattering grey gas (Floyd et al. 2003):

$$\vec{s}\times\nabla I(\vec{x},\vec{s}) = \kappa(\vec{x})[I_b(\vec{x},\vec{s}) - I(\vec{x},\vec{s})] \quad (12)$$

where $I(\vec{x},\vec{s})$ is the radiation intensity, $I_b(\vec{x},\vec{s})$ stands for the blackbody radiation intensity, $\kappa(\vec{x})$ is the absorption coefficient and $\vec{s}$ is the unit normal direction vector. The equation is solved using the finite volume method which divides all possible direction vectors ($\vec{s}$) into a number of solid angles. In the present investigation, the number of solid angles has been initially set to 104 (default value) and the sensitivity of the results to this parameter will be examined.

In LES models, physical processes (e.g. dissipative processes such as viscosity) which occur on length scales smaller than the numerical grid are modelled. To implicitly account for the effect of the subgrid scale physics upon the resolved scale of the flow, the Smagorinsky model of the eddy viscosity parameter is used:

$$\mu_{LES} = \rho(C_s\Delta)^2\left(2\bar{\bar{S}}_{ij}\cdot\bar{\bar{S}}_{ij} - \frac{2}{3}\left(\nabla\cdot\bar{\bar{u}}\right)^2\right)^{\frac{1}{2}} \quad (13)$$

where ρ is the density, C_s stands for the Smagorinsky constant (which is the only empirical parameter in the Smagorinsky model), Δ is a length on the order of the size of a grid cell (Eq. (14)) and S is the rate of strain tensor (the over bar "–" means that these are resolved values). The Smagorinsky constant usually takes value ranging from 0.1 to 0.2 and in the FDS code C_s is given a default value of 0.2. However, the sensitivity of the results to this parameter will not be examined as there is evidence that LES results are relatively insensitive to small variations in the value of the constant (Clement 2000).

1.2.2 Running the FDS model

FDS requires that all the necessary information to run the investigated case is supplied in the form of a single text file (a detailed description of the model and of its syntax may be found in the programme accompanying documentation (McGrattan et al. 2010a)).

The first command lines usually describe the computational domain and the desired spatial resolution. By default, grid cells are evenly spaced. Mesh size has a direct impact on the level of the geometric detail of the simulation as all solid objects have to be specified in terms of rectangular blocks which are forced to conform to the underlying computational grid. Grid resolution also affects the accuracy of the predictions through the filtering procedure which is intrinsic to the LES approach. Filtering refers to the mathematical operation intended to decompose the generic flow field property into a component which is explicitly solved for and a subgrid component which is modelled (Wang et al. 2002). The filter width Δ (i.e. the smallest scale of the resolved field) depends on the local mesh configuration as it is defined as follows:

$$\Delta = \left(\Delta x\Delta y\Delta z\right)^{1/3} \quad (14)$$

where Δx, Δy and Δz stand for the grid spacing in the x, y and z directions, respectively. The effect of different grid sizes was investigated and results are presented in Section 3.1.

In general, boundary conditions consist of physical quantities which are known from experimental measurements or are calculated from a model by means of empirical expressions. Exemplary parameters that describe the given set of boundary conditions may include temperature, velocity components and heat flux magnitudes. A physical model consists of a mathematical description of the reality. For instance, a physical model is needed to describe the nature of the heat transfer that exists in the fluid domain under investigation. The uncertainty due to unknown experimental operating conditions and wrong assumptions may influence simulation results. Section 4 analyzes in detail the uncertainties associated with the influence of the exterior domain and the description of heat transfer between the simulator and the surroundings.

2 Model description and representation

The experimental data measured by Kato (2005) made it possible to test the capability of a simplified simulation

approach of reproducing the flow around a standing occupant in a displacement ventilated room. The selected case study has already been referenced to in a number of previous studies. Deevy (2006) considered three different levels of detail ranging from a simple cylinder to a detailed human like geometry. The number of nodes varied from 95 000 to 225 000; tetrahedral cells were used in the domain with prism layers next to solid surfaces for boundary layer modelling. It was concluded that the predictions of the flow away from the body were acceptable with all the levels of detail. The most simplified geometry was not able to capture the features of the flow in the region next to the occupant such as the velocity field above the head which needed a more realistic shape to be considered. The Menter shear stress transport (SST) was used in the study. Deevy and Gobeau (2006) analyzed two geometries of the occupant, a simplified one and a realistic one. Unstructured meshes were used and the number of nodes ranged from 80 000 to 122 238 with prism shaped cells used near solid surfaces. Simulations adopted the SST turbulence model. The simpler geometry was found to produce similar results to that which was closer to the benchmark manikin with the exception of the region closer to the body to conclude that for many applications a simplified human geometry is sufficient to model the body influence on the resulting airflow. In (Yang et al. 2007) three levels of mesh resolution were used and the total number of elements ranged from 351 000 to 2 500 000. The total number of prism layers used to capture the effects of the boundary layer correctly varied from 3 to 10. The shape of the model was detailed and the SST turbulence model was adopted. CFD results showed favourable agreement with experimental data and it was found that the fine geometric features of the model had great effects on radiation prediction. Deevy et al. (2008) used a total of 222 116 nodes to resolve the shape of the manikin, the wall jet and buoyancy driven flow near the body of the human simulator; grid type was unstructured and the geometry used for reproducing the human manikin was realistic. Ten prismatic cells were used next to solid surfaces to correctly resolve the near wall flow. An unsteady Reynolds-averaged approach and detached-eddy simulation (DES) were used in the simulations. It was concluded that numerical results are in better agreement with the experiments when a radiation model is included in the simulations. In (Sideroff and Dang 2008) four grids were investigated based on the number of triangles used to define the manikin geometry, the average y^+ value on the manikin surfaces and the grid type (i.e. with or without boundary layer prismatic cells). In particular, the finest grid consisted up to about seven million cells. Solutions were obtained using two RANS models (the standard k-ε and the Durbins' model) and the dynamic Smagorinsky LES turbulence model. It was found that several prism layers were required to sufficiently resolve the boundary layer around the human simulator. Alternatively, employing a strictly tetrahedral topology for the entire domain would have resulted in grids in excess of ten million cells. Srebric et al. (2008) significantly simplified the geometry of the human manikin as the human shape was described by means of cuboids. A 180 000 and a 655 000 control volume grids were used to calculate numerical results; simulations used k-ε, RNG k-ε and LVEL turbulence models. It was found that the simplified geometry was able to reproduce the measurements in a reasonable way even though significant influence of boundary conditions, shape and size of the simulator was determined. Yan et al. (2009) compared a human like model to different levels of simplification in reproducing the features of the human shape. Only half of the room which was used in the benchmark exercise was simulated by means of two computational domains. The grid numbers in the volume surrounding the geometry of the simulator ranged from 315 000 to 182 000 and simulations used the RNG k-ε turbulence model.

Based on literature review, it was possible to identify the following points. As the level of detail of the human simulator increases, a finer, generally unstructured, computational grid is required to describe the geometry under consideration. Where a detailed resolution of the boundary layer is desired, a greater mesh density near the human model is needed. Good agreement between numerical results and experiments requires appropriate physical modelling and boundary conditions. In particular, when a total heat flux condition is prescribed, the convection to radiation heat flux proportion resulted often a critical parameter.

To represent the geometry of the problem being investigated, there were two options. The first was to specify a sufficiently fine grid that would have allowed to transform the details of the human body into a Cartesian geometry in order to retain its main anatomical features. An example of this strategy is presented in (Abanto et al. 2004). This strategy was rejected and different simplifications in the human simulator geometries were investigated. Three models were elaborated with a level of complexity consistent with practical engineering problems. They ranged from a over simplified heated cuboid to a more detailed model including features such as "legs", "arms" and "head" in order to investigate the relevance of their inclusion in the simulation model.

As the performed investigation aimed at exploring the correlations between model simplification (in terms of geometry and mesh generation) and simulation accuracy, it followed that grid size was deliberately chosen so that the total running time was less than a day (simulations were performed on a 8 GB RAM, 2.8 GHz computer) in order to couple the simplified models to a relatively fast solution. The initial computational grid consisted of a single rectangular

structured mesh with a 0.05 m element size. The resulting total number of cells was 210 000 and mesh elements were isometric (every time step the Courant-Friedrichs-Lewy (CFL) number is computed in each mesh cell and the time step is automatically adjusted so that the maximum value of the CFL number can vary between 0.8 and 1.0 (McGrattan et al. 2010a)).

The computational domain and the ventilation openings characteristics are presented in Fig. 1. The computational domain has dimensions 3 m × 3.5 m × 2.5 m. The flow is three-dimensional and non isothermal. The inlet air enters the room horizontally from an opening having dimensions 0.4 m (y direction) and 0.2 m (z direction) located at floor level and centred on the y axis. A passive exhaust is located at the ceiling on the opposite wall; exhaust size is 0.3 m (y direction) × 0.3 m (z direction). Supply velocity and temperature were 0.182 m/s and 21.8℃ respectively. A uniform velocity and temperature profile was assumed at the inlet (Deevy (2006) reported that the effect of changing the inlet conditions to those used in the experiments was tested and it was found to be negligible. A uniform profile for inlet velocity was assumed in (Yan et al. 2009) and good agreement between numerical results and measurements was observed). The human simulator, placed in the centre of the chamber 5 cm above the floor, is standing and facing the supply flow.

The experimental simulator adopted in the benchmark test was 1.66 m high and the total body surface area was 1.47 m^2. As regards the present study, the basic simulator (Shape 01) consisted of a single rectangular box; a more detailed simulator (Shape 02) included a gap between the legs (which was already identified to be important by Brohus and Nielsen (1996)) and a larger rectangular box representing the upper part of the body. A more complex geometry (Shape 03) was built including arms and a rectangular box representing the head. The FDS orthogonal grid did not allow for a precise replication of the benchmark model in the numerical simulations. However, the specific dimensions of the three investigated geometries were determined in order to reproduce as close as possible the features of the experimental simulator. The total exposed area of all the models was approximately identical (1.42 m^2 for the "Shape 01" and "Shape 02" models; 1.48 m^2 for the "Shape 03" geometry). All the models are 1.70 m high (z dimension). Figure 2 shows the different levels of detail used for the human simulator and Table 1 summarizes the corresponding most relevant features.

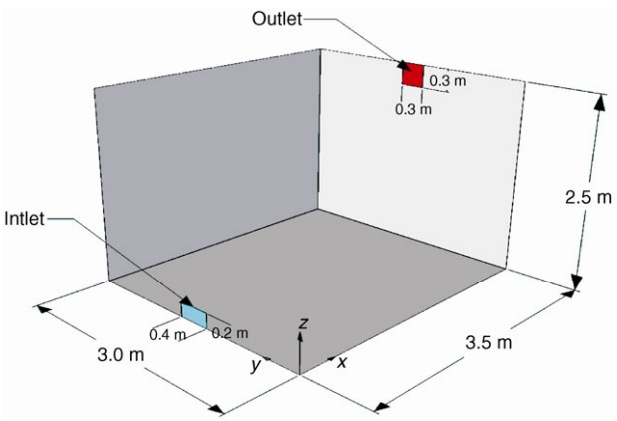

Fig. 1 3D visualization of the investigated displacement ventilated room

As to the thermal boundary conditions, the benchmark test prescribes the total heat loss from the manikin to the surroundings (76 W) without any prescriptive ratio about the relative proportions of convection and radiation being imposed. Srebric et al. (2008) recommended a convection to radiation ratio 30:70 for such simulations. Sideroff and Dang (2008) concluded that the actual radiative to convective heat transfer ratio should be 60:40. To further investigate the question, the actual fractions due to each of the two heat transfer mechanisms were computed numerically using an FDS feature which allows the user to specify a heat flux per unit surface area (kW/m^2) so that FDS consequently computes

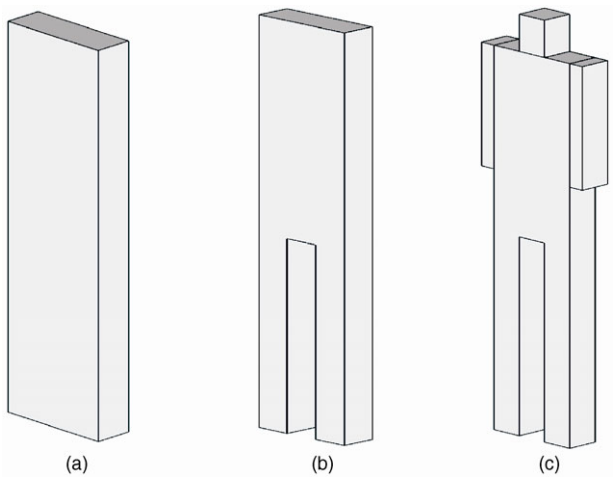

Fig. 2 Visualization of the three different representations for the human simulator considered in the analysis: (a) Shape 01; (b) Shape 02; (c) Shape 03

Table 1 Geometric details of the three representations of the human simulator considered in the analysis

	Shape 01	Shape 02	Shape 03
Torso	0.3 × 0.1 × 1.7	0.3 × 0.1 × 0.9	0.3 × 0.1 × 0.75
Legs	—	0.1 × 0.1 × 0.8	0.1 × 0.1 × 0.8
Head	—	—	0.15 × 0.1 × 0.15
Arms	—	—	0.05 × 0.1 × 0.50
Exposed area	1.42 m^2	1.42 m^2	1.48 m^2
Specific heat flux	53.5 W/m^2	53.5 W/m^2	51.4 W/m^2

All dimensions are specified in terms of (y axis)m × (x axis)m × (z axis)m

the surface temperature required to ensure that the combined net radiative and convective heat flux from the surface is equal to the imposed heat flux (McGrattan et al. 2010a). The specific heat flux was determined based on the total heat loss from the occupant (76 W) and its surface area so that the corresponding heat fluxes were 53.5 W/m^2 for the "Shape 01" and "Shape 02" models and 51.4 W/m^2 for the "Shape 03" model. The human simulator, walls, floor and ceiling of the computational domain were given a uniform emissivity of 0.9 (it was an approximate value which is common to most building surfaces and was assumed to apply for the human simulator too). Initial conditions considered quiescent air at 25℃ and room walls were assumed adiabatic.

3 Results

CFD simulations were performed and results were compared to experimental data. In the benchmark experiment measurements were conducted along four vertical poles, two in front (L1, L2) and two behind (L4, L5) the human simulator. For each pole, temperature measurements were performed at seven different heights and air velocities were evaluated at six sampling points (Fig. 3). Numerical results were calculated and compared at the same locations where experimental data were measured. No estimates of uncertainty or error were provided along with experimental data. Qualitative agreement with the experimental findings was assessed by comparing experimental and numerical temperature and velocity profiles at the selected vertical measuring poles. To quantitatively evaluate the accuracy of numerical results, root mean square residuals (RMS) were calculated as follows:

$$\mathrm{RMS} = \sqrt{\frac{\sum\left(y_{\mathrm{exp}} - y_{\mathrm{num}}\right)^2}{N}} \tag{15}$$

where N is the number of data points (i.e. $N = 7$ for temperatures, $N = 6$ for air velocities), y_{num} stands for the simulated value and y_{exp} for the corresponding measured value.

The time-average effect is a key point in explaining FDS results. Benchmark results make reference to steady state condition. Steady state condition is time independent whilst FDS simulations are inherently transient so that it was not possible to characterize the flow directly based on instantaneous flow properties as these were significantly affected by time dependent fluctuations. FDS simulations were run long enough so that they were not influenced by initial conditions (a 20 000 s period was simulated) and then results were averaged over a period long enough to smooth out time-dependent variations. The time period used for time averaging was determined based on the difference

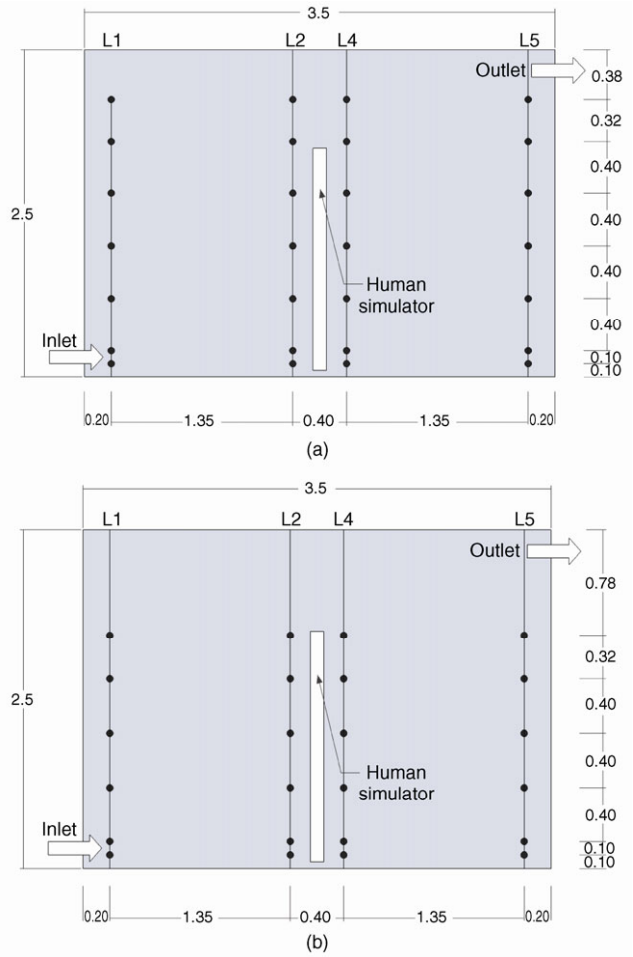

Fig. 3 Arrangement of the benchmark experimental sampling locations: (unit: m) (a) air temperature; (b) air velocity

between different averages at successive times. Sufficiently uniform temperature and air velocity profiles were generated by averaging over periods of 5000 s after the first 10 000 s of simulation time (data were collected at 1 s interval). To quantitatively transpose the requirement that by comparing various averaging periods nearly identical results had to be obtained, the maximum allowable temperature variation between any point in two successive profiles was determined in 0.1℃ and the maximum allowable variation in velocity was 0.01 m/s. As to the averaging procedure, although Jiang et al. (2003) found that the longer the averaging time is, the more accurate results are, however the adopted averaging period was significantly longer than those used in previous studies (600 s in (Emmerich and McGrattan 1998); up to 1500 s in (Musser et al. 2001)). The 5000 s averaging period resulted necessary to have undifferentiated temperature and velocity profiles as simulation results were affected by unsteady phenomena particularly in the regions near the human simulator. This behaviour is consistent with the results of (Deevy et al. 2008) which showed that, despite the use of constant boundary conditions, the mean flow around

the body was still observed to be unsteady. Moreover, Deevy (2006) found that unsteady effects were significant in the wake region behind the manikin. In particular, the present investigation showed a significant difference between temperature and air velocity in the averaging periods needed to characterize the flow. Figure 4 presents the temperature and velocity profiles generated by averaging data over periods of 1500 s; as regards temperature, there is not any significant difference between two successive periods. As regards air velocity, it can be seen how 1500 s averages at successive times yield different results (it is to note that the benchmark experiment is characterized by very low velocities; the meaning of "different" has to be interpreted in the light of the speeds involved).

Figures 5, 6 and 7 report the calculated temperature and velocity profiles. Based on the presented comparisons, there is not any significant difference between the two last periods (10 000 s – 15 000 s and 15 000 s – 20 000 s) considered in the analysis (for comparative purposes the period from 0 s to 5000 s is also shown). Table 2 reports the maximum temperature and air velocity differences between successive 5000 s averaging periods. Based on the assumed thresholds for temperature (0.1℃) and velocity (0.01 m/s), it can be concluded that the 20 000 s simulation period was necessary to characterize the flow for all the three geometries considered in the analysis.

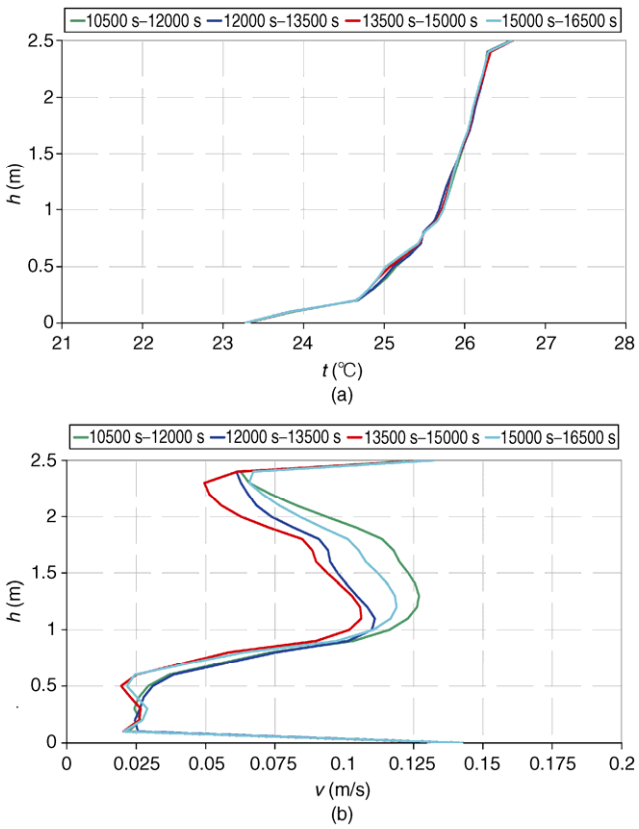

Fig. 4 Comparison of temperature (a) and velocity (b) profiles generated averaging data over 1500 s periods. Presented results refer to the L2 sampling pole

The qualitative agreement between numerical results and the benchmark data was acceptable. Comparing the resulting overall RMS residuals (Table 3 and Table 4), there is not appreciable difference in the overall simulation accuracy by using different geometries for the human simulator. In more details, as to the global field (i.e. the regions which are far most from the simulator) similar predictions were observed. In the region near the manikin some differences did occur. Figures 4(b), 5(b) and 6(b) present the velocity profiles in front of the human simulator; unexpectedly, the velocity predictions with the most simplified geometry resulted closer to the experimental data than those with the other two geometries which over predicted velocity by as much as approximately 0.1 m/s.

In addition to the sampling points for temperature and velocity, benchmark data provide also velocity distributions in the vicinity of the human simulator. The thermal plume from the occupant was a significant feature of the airflow in the room as the measured velocities above the occupant (the

Table 2 Maximum differences in temperatures (Δt) and air velocities (Δv) between successive 5000 s periods for the three shapes of the human simulator considered in the analysis

	Shape 01		Shape 02		Shape 03	
Simulation time (s)	Δt (℃)	Δv (m/s)	Δt (℃)	Δv (m/s)	Δt (℃)	Δv (m/s)
(0–5000) and (5000–10000)	0.213	0.028	0.238	0.023	0.233	0.015
(5000–10000) and (15000–10000)	0.018	0.004	0.032	0.014	0.025	0.004
(20000–15000) and (15000–10000)	0.016	0.003	0.016	0.003	0.03	0.008

Table 3 Temperature RMS at the different experimental sampling locations resulting from using different shapes for the human simulator

	Air temperature RMS residual (℃)			
Geometry	x = 0.20 m	x = 1.55 m	x = 1.95 m	x = 3.30 m
Shape 01	0.567	0.729	0.663	0.598
Shape 02	0.490	0.479	0.567	0.514
Shape 03	0.493	0.503	0.576	0.519

Table 4 Air velocity RMS at the different experimental sampling locations resulting from using different shapes for the human simulator

	Air velocity RMS residual (m/s)			
Geometry	x = 0.20 m	x = 1.55 m	x = 1.95 m	x = 3.30 m
Shape 01	0.015	0.020	0.018	0.020
Shape 02	0.015	0.066	0.022	0.015
Shape 03	0.015	0.059	0.019	0.015

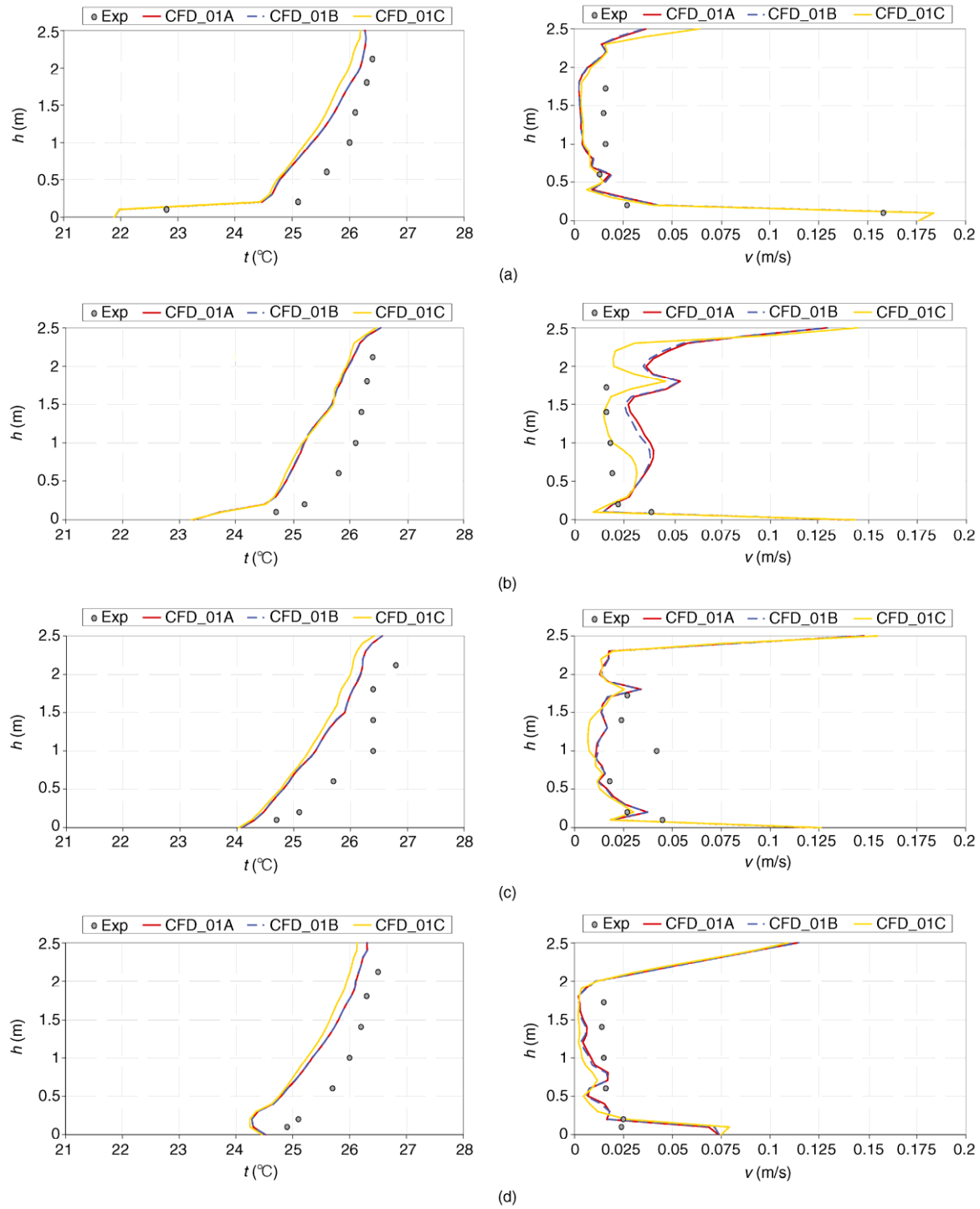

Fig. 5 Comparison between simulated and experimental temperature (t) and air velocity (v) profiles: (a) x = 0.20 m; (b) x = 1.55 m; (c) x = 1.95 m; (d) x = 3.3 m. As to the human simulator, presented results make reference to the "Shape 01" model (Exp = experimental data; CFD_01A = numerical results averaged between 10000 s–15000 s; CFD_01B = numerical results averaged between 15000 s–20000 s; CFD_01C = numerical results averaged between 0 s–5000 s)

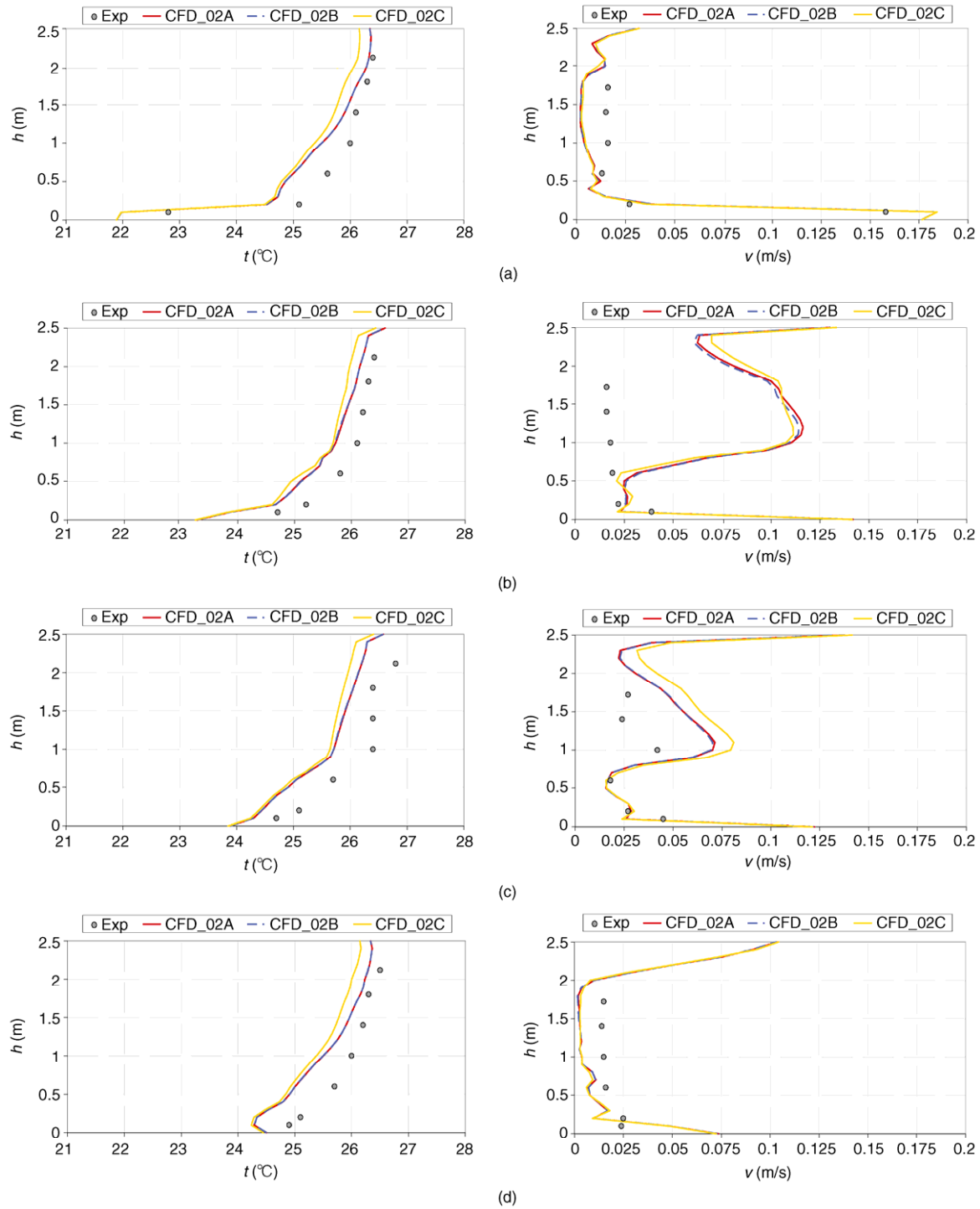

Fig. 6 Comparison between simulated and experimental temperature (t) and air velocity (v) profiles: (a) x = 0.20 m; (b) x = 1.55 m; (c) x = 1.95 m; (d) x = 3.3 m. As to the human simulator, presented results make reference to the "Shape 02" model (Exp = experimental data; CFD_02A = numerical results averaged between 10000 s–15000 s; CFD_02B = numerical results averaged between 15000 s–20000 s; CFD_02C = numerical results averaged between 0 s–5000 s)

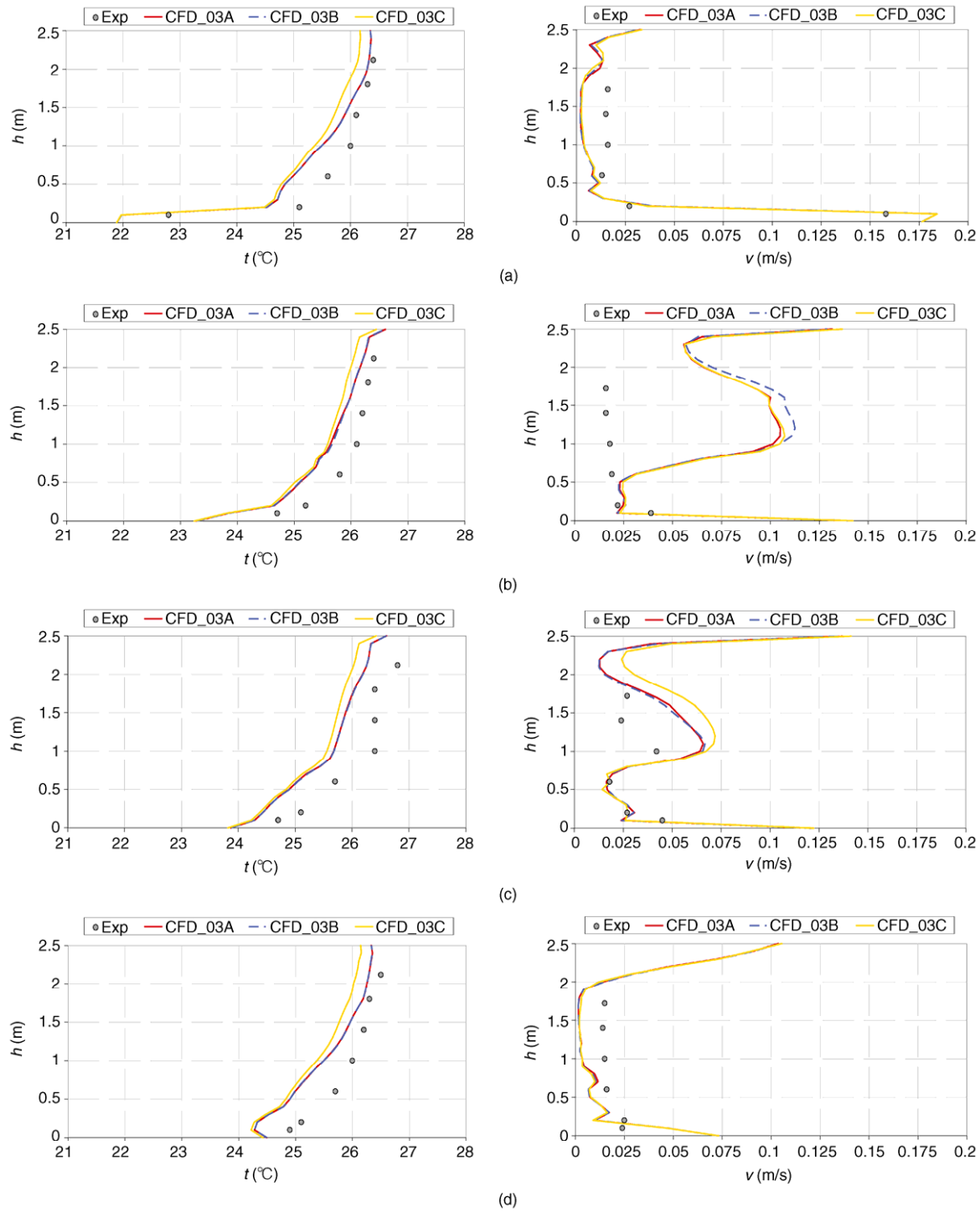

Fig. 7 Comparison between simulated and experimental temperature (t) and air velocity (v) profiles: (a) x = 0.20 m; (b) x = 1.55 m; (c) x = 1.95 m; (d) x = 3.3 m. As to the human simulator, presented results make reference to the "Shape 03" model (Exp = experimental data; CFD_03A = numerical results averaged between 10000 s–15000 s; CFD_03B = numerical results averaged between 15000 s–20000 s; CFD_03C = numerical results averaged between 0 s–5000 s)

peak overhead velocity was approximately 0.2 m/s) resulted of the same order of magnitude as those at the inlet. The simulator geometry and its excess temperature played a role in determining the resulting plume characteristics. Simulator surface temperatures (i.e. the "skin" temperature) were recorded and averaged between 15 000 s and 20 000 s of simulation time. The resulting mean temperature resulted approximately the same for all the three geometries: 32.6℃ for the "Shape 01" model, 33.1℃ for the "Shape 02" model and 32.9℃ for the "Shape 03" model. However, the temperature distribution around the mean value resulted different. For the "Shape 01" geometry, minimum (31.7℃) and maximum temperatures (33.0℃) were very close. As regards the "Shape 02" and the "Shape 03" geometries, the lower part of the "torso" as well as the two inner surfaces of the "legs" were significantly at a higher temperature. The effect of the inclusion of the "legs" resulted significant and it can be explored by looking at Fig. 8. Presented results refer to the "Shape 01" and "Shape 02" models (the "Shape 03" geometry is omitted as it was found to be very similar to the "Shape 02" one). The thermal plume caused by the human simulator and the floor jet that results from the incoming flow are clearly observed. However, the qualitative features of velocity contours are different as an increase in the upward velocity in the region around the human simulator is clear. By using the "Shape 01" model, a convective thermal plume took place uniformly along the entire body; the plume rises but without any lateral diffusion. By using the "Shape 02" geometry, heat rejection from the "legs" and the lower part of the "torso" in conjunction with the space between the two "legs" resulted in the entrainment of air from a higher horizontal distance from the body.

Relative proportions between convective heat transfer and radiative heat transfer are presented in Table 5. It is interesting to note that the calculated radiative to convective heat transfer ratios varied with height and all the geometries returned similar results. The radiation/convection proportions were approximately 70:30 for the upper portion of the models (i.e. "head", "torso" and "arms"), being equal to 60:40 for the lower part (i.e. "legs") which was characterized by stronger convection. The average convective heat transfer coefficient resulted approximately 2.5 W/(m²·K) for all the three shapes of the human simulator considered in the comparison.

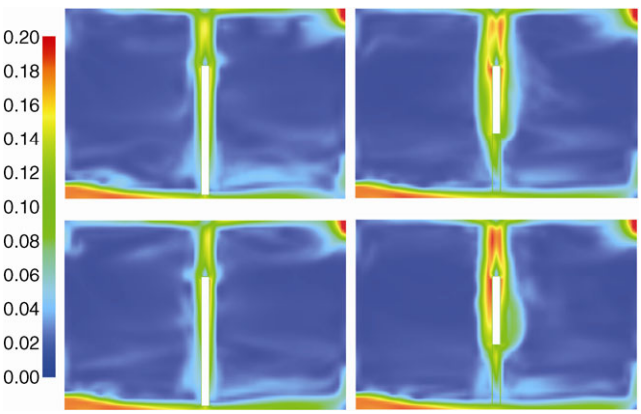

Fig. 8 Velocity (m/s) distribution at the symmetry plane (y = 1.5 m) with reference to two different levels of simplification of the human geometry: "Shape 01" model (left column) and "Shape 02" model (right column). Pictures refer to 16 000 s and 20 000 s of simulation time

Based on the simulations results, the following points were recognized.

The agreement between numerical results and the benchmark data was acceptable but not excellent. The qualitative trends seen in the benchmark experimental were captured but, as regards temperatures, numerical predictions resulted systematically far from the corresponding benchmark values. As regards air velocities, noticeable differences between simulated and measured data occurred in the regions near the simulator (in particular, if percentage differences are considered, the discrepancy often exceeds 100%. Even if relatively large percentage differences can be expected with low velocities, such a systematic large error suggests that, rather than being an isolated perturbation, the problem had probably to be extended to the input leading to it).

In ambient air with speed less than 0.1 m/s and standing posture, mean convective heat transfer coefficients of a human body were reported varying in the range from 3.4 W/(m²·K) to 4.3 W/(m²·K) (Gao and Liu 2005). Yang et al. (2007) reported CFD predictions varying from 3.9 W/(m²·K) to 4.3 W/(m²·K). As to the simulations, the predicted convective heat transfer coefficients resulted noticeably lower than the

Table 5 Calculated ratios between radiative heat transfer ("*Rad*") and convective heat transfer ("*Conv*") for the three geometries of the human simulator considered in the analysis

		Shape 01		Shape 02		Shape 03	
		Rad	*Conv*	*Rad*	*Conv*	*Rad*	*Conv*
Torso		52.5 (69.1%)	23.5 (30.9%)	29.0 (71.2%)	11.7 (28.8%)	19.2 (70.6%)	8.0 (29.4%)
Legs	Left	—	—	9.9 (56.1%)	7.7 (43.9%)	9.5 (56.2%)	7.4 (43.8%)
	Right	—	—	10.8 (61.4%)	6.8 (38.6%)	10.4 (61.4%)	6.5 (38.6%)
Head		—	—	—	—	2.6 (71.7%)	1.0 (28.3%)
Arms	Left	—	—	—	—	4.0 (70.8%)	1.6 (29.2%)
	Right	—	—	—	—	4.0 (70.9%)	1.6 (29.1%)

"Left" and "Right" make reference to the human simulator as seen from the coordinate system origin.

reported values. As to the distribution of skin surface temperature, the maximum value above 37℃ which resulted for the "Shape 02" (37.6℃) and "Shape 03" (37.2℃) models over predicts the temperature distribution depicted in (Kato and Yang 2006). Moreover, the average surface temperature exceed by as much as 1℃ ("Shape 02") than the benchmark value (32.2℃). Even if the emissivity of the simulator geometry was initially set to unity, Doherty and Arens (1988) reported skin emissivity estimations should vary between 0.97 and 1.

Based on the above discussion, it was concluded that the models used in the numerical simulations may have included some inaccuracies due to the assumptions made in their development:

(1) Grid resolution. The computational setup aimed at simplifying the problem under investigation; this could have been at the expense of accuracy. More nodes next to the human simulator could have been required to capture the patterns of air velocities. Hence, to investigate the influence of spatial resolution on simulation accuracy and computing times several grids were further analyzed.
(2) The influence of the exterior environment. The benchmark experimental setup makes reference to adiabatic walls. In (Srebric et al. 2008) additional 10 W were added due to the heat transferred through the walls. To explore the influence of the heat transfer from the room envelope, the adiabatic room assumption was revised.
(3) FDS solves the governing equations on a rectilinear grid and all solid objects have to be specified in terms of rectangular blocks so that it resulted necessary to represent a complex geometry (e.g. the human torso) by means of a single box approximation. As sharp edges may have implications on the resulting flow features, the effect of the box-like geometry was studied.
(4) Heat transfer coefficients and surface temperature distribution. Skin temperatures are essential in determining the density gradients driving the plume around the occupant. The influence of skin emissivity and body mean convective heat transfer coefficient was further investigated in order to evaluate their effect on the surface temperature distribution, on the mechanisms of the sensible heat transfer from the simulator surfaces to the surroundings and on the development of the thermal plume.

The relevance of these aspects was further investigated by performing different adjustments to the initial simulation setup. The gap between the "legs" resulted a geometrical feature much more significant than the inclusion of the "head" and the "arms" as it played a role in the development of the thermal plume above the occupant and in the definition of the horizontal distance impacted by the presence of the simulator. Therefore, the "Shape 01" and "Shape 03" geometries were excluded from further numerical experiments with modified inputs which considered the "Shape 02" model as the baseline case.

3.1 Effect of the spatial resolution of the computational grid

This paper presents an approach to indoor airflow simulation based on relatively coarser grids than those which are usually used for such simulations. The differences between numerical results and measurements could have determined by the adopted spatial resolution. In order to address the effect of grid spatial resolution, four grids were compared and the difference in the predictions was assessed by comparing the corresponding results with experimental data at the different sampling locations. The coarsest cell size was 0.05 m × 0.05 m × 0.05 m; the finest grid represented the domain by 840 000 cells with dimensions 0.025 m × 0.025 m × 0.025 m (with reference to the latter case, since the room is geometrically symmetrical, only half of the chamber was simulated). Grid details are summarized in Table 6 where it is to note that cases ID "B" and "C" make use of non isometric elements. FDS allows the cells to be non uniform in one or two of the three coordinate directions. Due to the flow peculiar directionality, element transformations were firstly performed in the x axis (floor jet entering the room) and z axis (thermal plume above the human simulator). For comparison purposes, mesh transformation was repeated in the x axis and z axis. Boundary conditions were not modified.

In general, the more detailed the grid resolution the more precise results are supposed to be (Li and Yang 2009). Mesh size has also significant implications on the required solution times as, by increasing the number of nodes, higher computing times are expected. In general, the use of a non isometric mesh enables to reduce the total number of elements in the flow domain by reducing mesh spacing exclusively in the regions where it is supposed it is needed most. However, non isometric mesh elements may be responsible of numerical errors into the simulation thus affecting the accuracy of the results (Hadjisophocleous and McCartney 2005).

Simulations were run for 20 000 s and the 5000 s averaging period was maintained. Results are presented in Fig. 9. It can

Table 6 Summary of the different grid spacing used to test the effect of mesh spatial resolution (resolution is expressed in terms of number of cells in the x, y and z directions)

Case ID	Resolution	Transform type	Grid resolution (m)
A	70 × 60 × 50	None	0.05 × 0.05 × 0.05
B	140 × 60 × 100	x-axis; z-axis	0.025 × 0.05 × 0.025
C	140 × 120 × 50	x-axis; y-axis	0.025 × 0.025 × 0.05
D	140 × 60 × 100	None	0.025 × 0.025 × 0.025

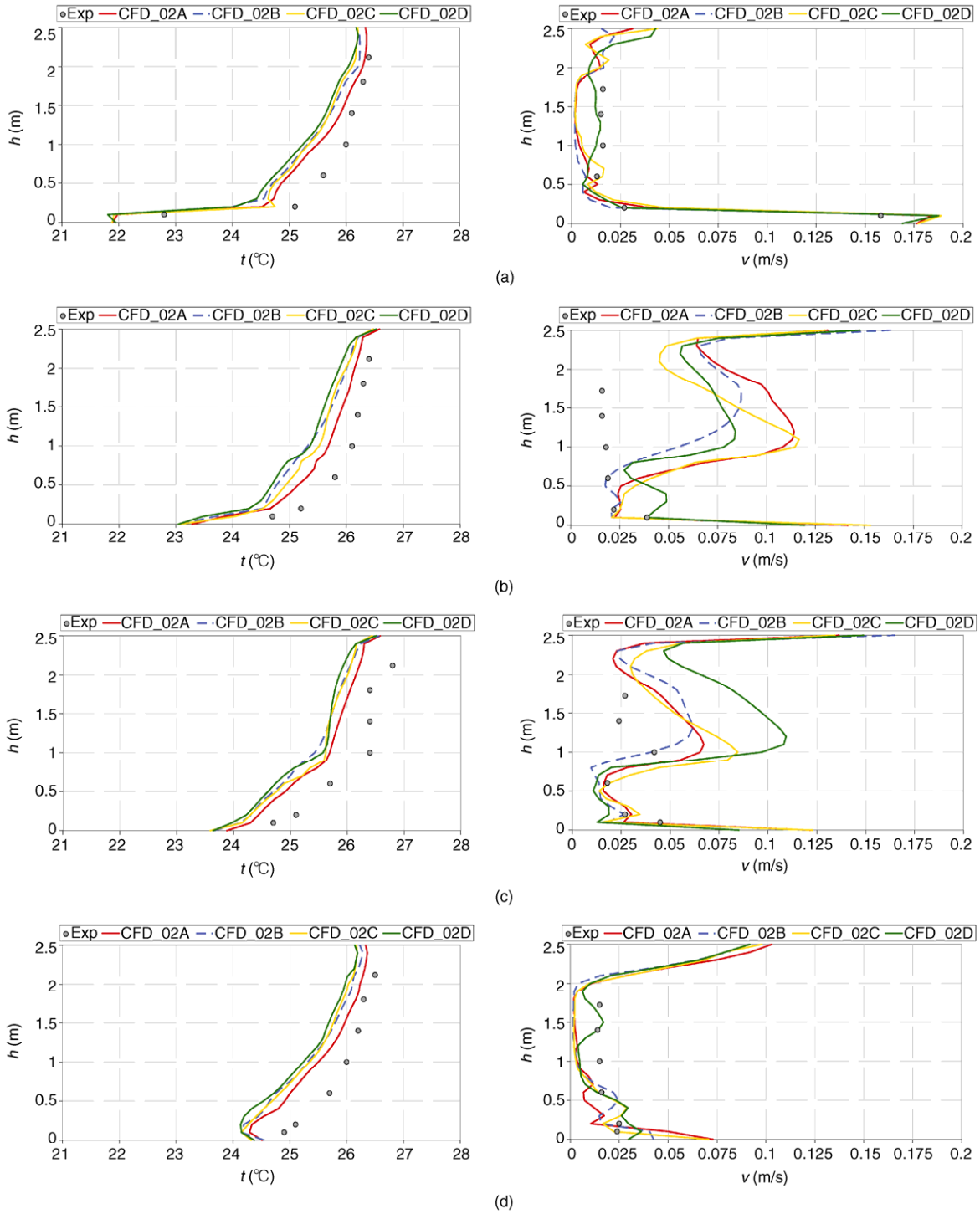

Fig. 9 Comparison between simulated and experimental temperature (t) and air velocity (v) profiles: (a) x = 0.20 m; (b) x = 1.55 m; (c) x = 1.95 m; (d) x = 3.3 m. (Exp = experimental; CFD_02A = 0.05 m isometric grid; CFD_02B = 0.025 m × 0.05 m × 0.025 m grid; CFD_02C = 0.025 m × 0.025 m × 0.05 m grid; CFD_02D = 0.025 m isometric grid)

be seen that the profiles produced by the different grids considered in the investigation do not differ significantly, especially as to the regions far from the human simulator (i.e. poles L1 and L5). Moreover, it is to note that the two non isometric grids returned similar results. Temperature was generally not very sensitive to grid size. Instead, there were more variations in the air velocity profiles generated using different levels of grid refinement. As to poles L1 and L5, all the grids did appear to be converging to a common profile. On the contrary, with reference to poles L2 and L4, they did not. As to them, results showed a general trend where the most notable feature is the velocity increase between 1.0 m and 1.5 m from the floor. Agreement with experimental data was generally not better than that which was obtained by using a coarser grid (0.05 m). For comparison purposes, simulation took 15 hours for the 0.05 m isometric grid; total computing times were 168 hours for the 0.025 m isometric grid. The two non isometric grids required 219 and 232 hours respectively to conclude that mesh transformations did not result in any significant improvement in the accuracy of the predictions.

Based on the above results it was concluded that the reason for the lack of agreement between numerical results and measurements probably lied in the adopted boundary conditions. Therefore, some of the input parameters were better calibrated in order to tune the model to measured data.

4 Model improvement and calibration

Potential sources of discrepancies in the CFD results may result from boundary conditions in the case they do not correspond exactly with those in the experiments. Boundary conditions which were recognized of having a significant effect on the model output were identified and then successive adjustments were performed to reproduce experimental conditions more closely. The final model was created and results are presented.

Although the benchmark test prescribes walls to be adiabatic, neglecting the heat transfer from walls may have some implications on room air temperature and on simulator surface temperatures. Based on the discussion presented in (Srebric et al. 2008), an additional heat flux (10 W) was introduced in the computational domain to account for the heat conduction through the room envelope. The supplemental 10 W heat flux (rather than being forced to be pure convection) was imposed on the floor taking advantage of the above mentioned FDS feature which allows the prescription of a total heat flux being the radiative and convective fraction computed numerically.

The "a priori" selection of a convective heat transfer coefficient is not an easy task but it can have a significant impact on the results generated by the simulation (Musser et al. 2001). In the case of ambient air speeds lower than 0.2 m/s air movement is driven purely by natural convection (De Dear et al. 1996). The default values used in FDS for determining the convection coefficients (i.e. the "*C*" term in Eq. (11)) are taken from (ASHRAE 2001) which gives 1.31 and 1.52 for large vertical plates and for large horizontal plates respectively (however, it is cited that caution should be used when transposing these relationships from vertical plates to vertical surfaces in enclosed spaces). FDS allows the user to specify a convection coefficient for each of the surfaces composing the computational domain. A constant coefficient of 3.9 W/(m^2·K) was imposed on all the surfaces of the human simulator (the value was chosen to fall within the mid range of previously published values varying from 3.4 W/(m^2·K) to 4.3 W/(m^2·K)). The simulator surface emissivity was also set to unity.

FDS makes available an optional control (i.e. the "SAWTOOTH" parameter) to lessen the impact of vortices at sharp corners due to the parallele-piped boxes necessarily used to represent non rectangular objects. By using this feature vorticity is imposed to zero at the corners of the generic obstruction in order to reduce potential errors due to artificially increased entrainment and drag (from a mathematical stand point, the "SAWTOOTH" option turns off the vorticity term in the momentum equation). The above described vorticity compensation was imposed on the block composing the upper part of the human simulator (i.e. the "torso").

Results are presented in Fig. 10. A higher skin emissivity and a higher convection coefficient resulted in lower surface temperatures: minimum, average and maximum values were, respectively, 30.8℃, 32.2℃, and 36.8℃ (for comparison purposes, the temperature distribution with the initial model resulted in 31.8℃, 33.1℃, and 37.6℃ for the minimum, average and maximum values). The average value resulted to match the benchmark simulator average surface temperature. The maximum temperature was recorded at the "groin" level; although 36.8℃ was the lowest value among all the simulated cases, it still resulted higher than the value reported in (Kato and Yang 2006).

With reference to air velocity, the combined effects due to the surface temperature decrease and to the vorticity compensation option resulted in a reduction of the horizontal distance impacted by the presence of the occupant. As to poles L2 and L4, it is to note that the predicted velocity resulted smoother (i.e. the profile is less perturbated by the presence of the human simulator). Tables 7 and 8 summarize the resulting RMS residual results where it can be seen a general reduction of the errors with reference to the initial "Shape 02" model which was the baseline model for the comparison. The details about the proportions between the convective heat transfer and the radiative heat transfer are summarized in Table 9. It is interesting to note that the

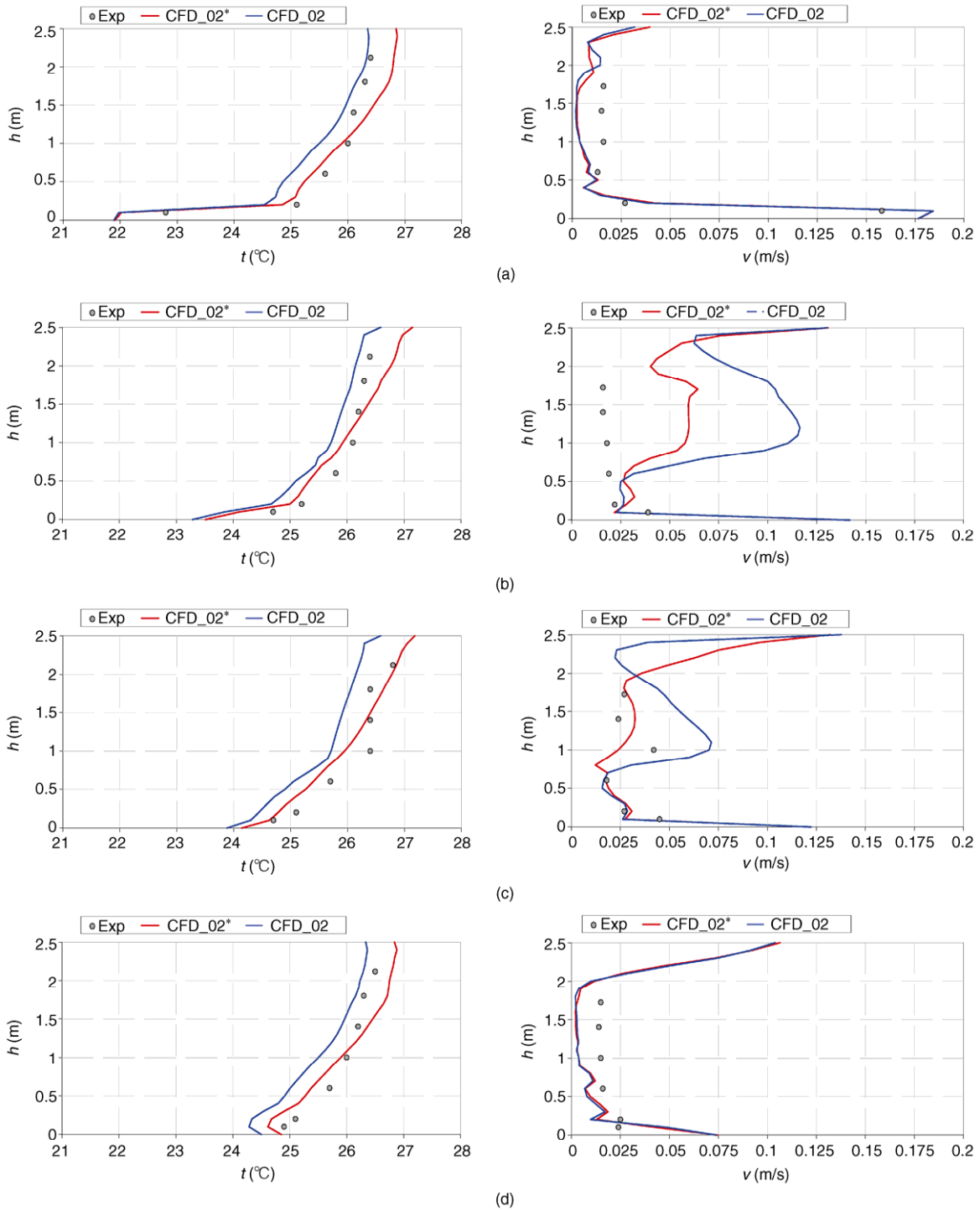

Fig. 10 Comparison between simulated and experimental temperature (t) and air velocity (v) profiles: (a) x = 0.20 m; (b) x = 1.55 m; (c) x = 1.95 m; (d) x = 3.3 m. (Exp = experimental; CFD02 = initial "Shape 02" model; CFD02* = adjusted "Shape 02" model as described in Section 4)

Table 7 Comparison between the temperature RMS at the different sampling locations resulting from the adjustment of boundary conditions (results in brackets refer to the initial model; the results above refer to the model as described in Section 4)

	Air temperature RMS residual (℃)			
Geometry	x = 0.20 m	x = 1.55 m	x = 1.95 m	x = 3.30 m
Shape 02	0.405 (0.490)	0.346 (0.479)	0.256(0.567)	0.305 (0.514)

Table 8 Comparison between the air velocity RMS at the different sampling locations resulting from the adjustment of boundary conditions (results in brackets refer to the initial model; above the results referring to the model as described in Section 4)

	Air velocity RMS residual (m/s)			
Geometry	x = 0.20 m	x = 1.55 m	x = 1.95 m	x = 3.30 m
Shape 02	0.015 (0.015)	0.032 (0.066)	0.011 (0.022)	0.013 (0.015)

Table 9 Details on the heat flux from different segments of the human simulator after the skin emissivity "(*Rad*)" and body mean convective "(*Con*)" heat transfer, coefficient were revised (for comparison purposes, enclosed in parenthesis, the corresponding heat flux in the case of the initial model)

		Total (W)	*Rad*	*Conv*
Torso		40.7 [40.7]	26.2 (64.5%) [29 (71.2%)]	14.5 (35.5%) [11.7 (28.8%)]
Legs	Left	17.7 [17.7]	8.6 (48.6%) [9.9 (56.1%)]	9.1 (51.4%) [7.7 (43.9%)]
	Right	17.7 [17.7]	9.5 (53.8%) [10.8 (61.4%)]	8.2 (46.2%) [6.8 (38.6%)]

"Left" and "Right" make reference to the human simulator as seen from the coordinate system origin.

radiative to convective heat transfer ratio was approximately 70:30 for the upper part of the body whilst it was 50:50 for the two "legs". If the simulator is considered as a whole, it resulted that the total radiation heat loss accounted for 44.3 W and the total convective heat loss was 31.7 W, being the proportion 58.3% to 41.7%. This result is consistent with the general indication that, if low velocities are considered, between 60% and 49% of the sensible heat emission from a human being can be radiant depending on type of clothing and activity (ASHRAE 2005).

4.1 Effects of thermal radiation modelling

To test the sensitivity of results to radiation modelling three cases were compared with and without radiation modelling. For calculations involving radiation modelling, the same boundary conditions were used as those for the optimized model described in Section 4 and the number of solid angles used in the radiation model (Section 1.2.1) was altered from its default number (104) to 208. For comparison purposes, simulations were also repeated without radiation modelling. In this case, a 38 W heat flux was uniformly distributed on the exposed surface area of the simulator and the supplemental heat flux due to heat transfer from room floor was reduced to 5 W (convection only).

Figure 11 depicts temperature and air velocity contours around the human simulator. Based on the presented results, it was possible to draw the following conclusions. It was found that the resulting temperature distribution was noticeably lower in the case radiation was not included in the simulation. Airflow in a displacement ventilated enclosure is predominantly buoyancy driven so that capturing the correct temperature gradient is critical to the accurate prediction of room airflow. As radiation causes walls to heat up, the results without a radiation model returned an increased horizontal spreading of the floor jet because of the reduced floor temperature. Similar results can be found in (Deevy and Gobeau 2006). The 208 solid angle model was computationally more demanding; the 20 000 s simulation took about 29 hours in the case the default number of solid angles was used (the CPU time usage was 17%) and approximately 33 hours in the case it was altered to 208 (the CPU time usage was 28%). Despite the increase in the required computational resources, the 208 solid angle model returned very similar results to the default radiation model suggesting that, as to the investigated case, the latter approach is sufficient.

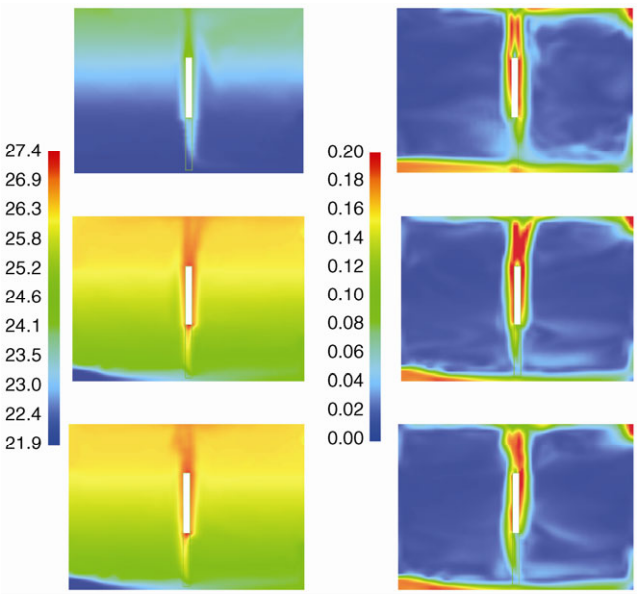

Fig. 11 Temperature (℃, left) and velocity (m/s, right) distribution at the symmetry plane (y = 1.5 m) in the case only convection is considered in the simulation (top), the model is as described in Section 4 (middle) and the number of radiation solid angles was altered to 208 (bottom)

4.2 The influence of the occupant

The present investigation moved its steps from the need of assessing in detail the interaction between occupants and room air. Although experimental data are not available and therefore a comparison is not possible, it seemed reasonable to use CFD to evaluate the impact the occupant had on the indoor temperature and air velocity distributions by assuming the room was empty (the supplemental 10 W heat flux was retained). Figure 12 presents the temperature and air velocity results evaluated at the L4 position averaged over 1000 s periods. It is interesting to note that results converged to a common profile much faster than in the case the room was occupied. The influence of the occupant was particularly significant on thermal loading as it resulted a significant decrease in the resulting temperature distribution. Moreover, the convection flow generated by the occupant was responsible of a marked spatial disuniformity in the velocity distribution which did not result in the case the room was assumed to be empty to conclude that, as to the investigated room, the occupant's influence was an essential feature of the resulting indoor airflow.

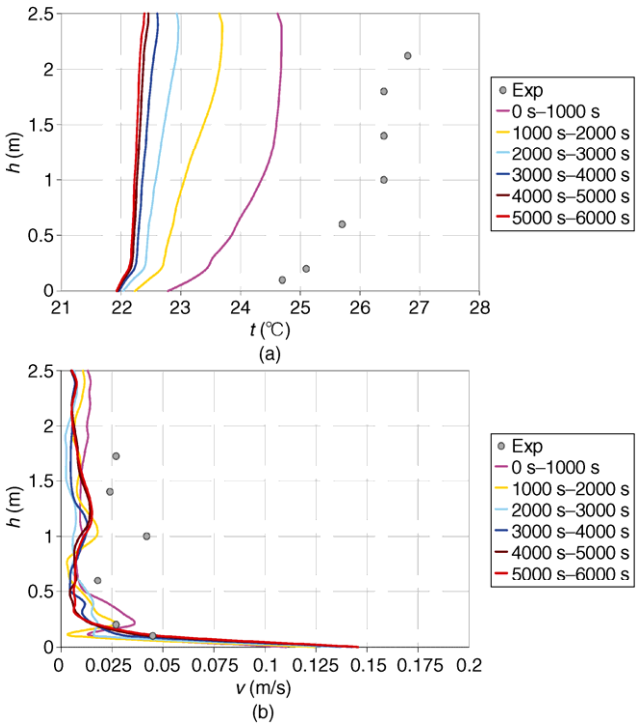

Fig. 12 Successive averages over 1000 s periods for temperature (a) and air velocity (b) in the case the room is considered to be empty. Presented results refer to the L4 sampling pole

5 Conclusions

A more realistic and accurate indoor airflow simulation is one that takes into account the combined effects of obstacles and heat sources. This puts higher demands on the simulation requirements. Simplified CFD models require reduced computing resources and provide faster results but the accuracy of predictions has to be carefully evaluated. To determine the potential use of a simplified simulation approach to predict the airflow and heat transfer around the occupant of a displacement ventilated room, this paper has presented the application of a computational model which combines simple geometry and mesh generation to a literature benchmark test case. Different simplifications of the human shape have been considered but all the investigated geometries were represented by means of box-like obstructions. A uniformly spaced Cartesian grid was adopted in the simulations. Numerical results and experimental data were then compared and strengths and weaknesses of the simplified approach were determined. Although the models were significantly simplified with reference to realistic, human like, simulators (often combined to densely packed grids near the surfaces) which have been used in previous similar studies, numerical results show that even a simplified model yield acceptable simulation results provided that some attention is paid to the inclusion of relevant geometric features such as the space between the two "legs" and to the definition of adequate boundary conditions.

The adopted simplified approach was reasonably able to reproduce spatial gradients in the room. As to the "Shape 02" geometry (as described in Section 4), the largest difference between predicted and measured temperatures is less than 1 K and the calculated average surface temperature matched the measured one. As to air velocity, the velocity patterns above the head of the occupant were also captured. The agreement between numerical results and measurements still resulted to be weakest in the proximity of the simulator, although the agreement has been improved with reference to the initial model. As to the requirements for a proper choice of the number of cells to be used in the simulations, the final "Shape 02" model simulation took about 29 h on a personal computer to be performed (including radiation modelling) to conclude that an optimized definition of the geometry, the physical models and boundary conditions makes it possible to ensure a trade off between simulation accuracy and grid resolution which is of particular interest for the cases which require solutions over large real times.

A CFD model for indoor airflow predictions was developed and the computational model was based on the Fire Dynamics Simulator (FDS) model. The comparison with experimental results and the successive adjustments which were performed to reconcile numerical predictions and measurements enabled to identify a number of issues important to FDS practitioners: (1) in indoor simulations dealing with non fire scenarios (i.e. for the cases where airflow is not dominated by a strong convective force as

with a large fire) local effects may have a significant impact on simulation predictions. For instance, skin temperatures had an impact on the plume development around the simulator. As to the convective heat transfer coefficients, calculated values should be compared to existing values to verify their appropriateness. (2) as to the presented case, the "SAWTOOTH" parameter enabled a better agreement between measurements and numerical predictions to suggest that it can be useful when simulating complex geometries such as the human body (nevertheless, the applicability has to be evaluated on a case by case basis).

However, it was not possible to completely conclude that accurate predictions of the details of the airflow field around a human body can be obtained apart from a more sophisticated representation of the human shape. The agreement on the airflow velocities was not completely satisfactory, especially in the vicinity of the occupant. More precise and complete results would have required a more complex mesh generation or the inclusion in the CFD model of more anatomical details of the human shape. As local airflow patterns will influence personal microclimate and personal exposure to contaminants, more detailed computational models are needed to address such investigations.

References

Abanto J, Barrero D, Reggio M, Hardy JP, Ozell B (2004). Application of CFD tools in building engineering and in fire simulation. Paper presented at the Simbuild Conference, University of Colorado, Boulder, USA.

ASHRAE (2001). ASHRAE Handbook—Fundamentals. Atlanta, USA: American Society of Heating, Refrigerating and Air-Conditioning Engineers.

ASHRAE (2005). ASHRAE Handbook—Fundamentals. Atlanta, USA: American Society of Heating, Refrigerating and Air-Conditioning Engineers.

Bolashikov ZD (2010). Advanced methods for air distribution in occupied spaces for reduced risk from airborne diseases and improved air quality. PhD Dissertation, Department of Civil Engineering, Technical University of Denmark, Denmark.

Brohus H (1997). Personal exposure to contaminant sources in ventilated rooms. PhD Dissertation, Faculty of Engineering and Science, Aalborg University, Denmark.

Brohus H, Nielsen PV (1996). CFD models of persons evaluated by full scale wind channel experiments. Paper presented at the 1996 RoomVent Conference, Japan.

Caciolo M, Stabat P, Marchio D (2012). Numerical simulation of single sided ventilation using RANS and LES and comparison with full-scale experiments. *Building and Environment*, 50: 202 – 213.

Clement JM (2000). Experimental verification of the Fire Dynamics Simulator (FDS) hydrodynamic model. PhD Thesis, University of Canterbury, New Zealand.

Cho YH, Liu M (2010). Correlation between minimum airflow and discharge air temperature. *Building and Environment*, 45: 1601 – 1611.

Craven BA, Settles GS (2006). A computational and experimental investigation of the human thermal plume. *Journal of Fluids Engineering*, 128: 1251 – 1258.

De Dear JR, Arens AE, Zhang H, Oguro M (1996). Convective and radiative heat transfer coefficients for individual human body segments. *International Journal of Biometeorology*, 40: 141 – 156.

Deevy M (2006). CFD modelling of the benchmark displacement ventilation test case. Health and Safety Laboratory, HSL0686.

Deevy M, Gobeau N (2006). CFD modelling of benchmark test cases for flow around a computer simulated person. Health and Safety Laboratory, HSL0651.

Deevy M, Sinai Y, Everitt P, Voigt L, Gobeau N (2008). Modelling the effect of an occupant on displacement ventilation with computational fluid dynamics. *Energy and Buildings*, 40: 255 – 264.

Doherty T, Arens AE (1988). Evaluation of the physiological bases of thermal comfort models. *ASHRAE Transactions*, 94 (1): 1371 – 1385.

Emmerich SJ (1997). Use of computational fluid dynamics to analyze indoor air quality issues. National Institute of Standards and Technology (NIST), NISTIR 5997.

Emmerich SJ, McGrattan KB (1998). Application of a large eddy simulation model to study room airflow. *ASHRAE Transactions*, 104(1): 1128 – 1137.

Farnham C, Nakao M, Nishioka M, Nabeshima M, Mizuno T (2011). Study of mist-cooling for semi-enclosed spaces in Osaka, Japan. *Procedia Environmental Sciences*, 4: 228 – 238.

Floyd JE, McGrattan KB, Hostikka S, Baum HR (2003). CFD fire simulation using mixture fraction combustion and finite volume radiative heat transfer. *Journal of Fire Protection Engineering*, 13: 11 – 36.

Gao N, Liu J (2005). CFD study of the thermal environment around a human body: A review. *Indoor and Built Environment,* 14: 5 – 16.

Hadjisophocleous GV, McCartney CJ (2005). Guidelines for the use of CFD simulation for fire and smoke modelling. *ASHRAE Transactions*, 111 (2): 583 – 594.

Hostikka S (2011). The FDS Road Map. Available: http://code.google.com/p/fds-smv/wiki/FDS_Road_Map.

Jiang J, Wang X, Sun Y, Zhang Y (2009). Experimental and numerical study of air flows in a full scale room. *ASHRAE Transactions*, 115(2): 867 – 886.

Jiang Y, Alexander D, Jenkins H, Arthur R, Chen Q (2003). Natural ventilation in buildings: Measurements in a wind tunnel and numerical simulation with large eddy simulation. *Journal of Wind Engineering and Industrial Aerodynamics,* 91: 331 – 353.

Kato S (2005). Displacement Ventilation: Comprehensive Experimental Data. Available: http://www.civil.auc.dk/%7Ei6pvn/cfd-benschmarks/csp_benchmark_test/.

Kato S, Yang JH (2006). Benchmark Tests of CFD Airflow Around Human Body in a Room with Displacement Ventilation. Available: http://www.civil.auc.dk/%7Ei6pvn/cfd-benschmarks/csp_benchmark_test/.

Li Q, Yang Q (2009). Comparison of subgrid-scale models in large eddy simulation of flow over a rectangular obstacle. Paper presented at the 7th Asia-Pacific Conference on Wind Engineering, Taipei, Taiwan, China.

Lin CH, Wu TT, Horstman RH, Lebbin PA, Hosni MH, Jones BW and Beck BT (2006). Comparison of large eddy simulation predictions with particle image velocimetry data for the airflow in a generic cabin model. *HVAC & Research*, 12: 953 – 951.

Liu W, Mazumdar S, Zhang Z, Poussou SB, Liu J, Lin CH, Chen Q (2012). State-of-the-art methods for studying air distributions in commercial airliner cabins. *Building and Environment*, 47: 5 – 12.

McDermott R (2009). FDS wall flows Part I: Straight channels. National Institute of Standards and Technology, NIST Technical Note 1640.

McDermott R, McGrattan K, Hostikka S, Floyd J (2010). Fire Dynamics Simulator (Version 5) Technical Reference Guide. Volume 2: Verification. National Institute of Standards and Technology (NIST) Special Publication 1018-5.

McGrattan K, McDermott R, Hostikka S, Floyd J (2010a). Fire Dynamics Simulator (Version 5) User's Guide. National Institute of Standards and Technology (NIST) Special Publication 1019-5.

McGrattan K, McDermott R, Hostikka S, Floyd J (2010b). Fire Dynamics Simulator (Version 5) Technical Reference Guide. Volume 3: Validation. National Institute of Standards and Technology (NIST) Special Publication 1019-5.

McGrattan K, Hostikka S, Floyd J, Baum H, Rehm R, Mell W, McDermott R (2010c). Fire Dynamics Simulator (Version 5) Technical Reference Guide. Volume 1: Mathematical Model. National Institute of Standards and Technology, NIST Special Publication 1018-5.

McGrattan K, McDermott R, Floyd J, Hostikka S, Baum H (2012). Computational fluid dynamics modelling of fire. *International Journal of Computational Fluid Dynamics*, 26: 349 – 361.

Mora L, Gadgil AJ (2002). Theoretical study of pollutant mixing in rooms induced by occupancy. Paper presented at the 2002 RoomVent Conference, Copenhagen, Denmark. Also Lawrence Berkeley National Laboratory Report LBNL-49730.

Musser A, McGrattan KB, Palmer J (2001). Evaluation of a fast, simplified computational fluid dynamics model for solving room airflow problems. National Institute of Standards and Technology (NIST), NISTIR 6760.

Sideroff CN, Dang TQ (2008). Verification and validation of CFD for the personal micro-environment. *ASHRAE Transactions*, 114(2): 45 – 56.

Shih N, Lee W (2004). Particles simulation and evaluation of personal exposure to contaminant sources in an elevation space. Paper presented at the 10th International Conference on Computing in Civil and Building Engineering, Weimar, Germany.

Srebric J, Vukovic V, He G, Yang X (2008). CFD boundary conditions for contaminant dispersion, heat transfer and airflow simulations around human occupants in indoor environments. *Building and Environment*, 43: 294 – 303.

Temmerman L, Leschzinger MA, Mellen CP, Fröhlich J (2003). Investigation of wall function approximations and subgrid scale models in large eddy simulation of separated flow in a channel with streamwise periodic constrictions. *International Journal of Heat and Fluid Flow*, 24: 157 – 180.

Wang HY, Coutin M, Most JM (2002). Large eddy simulation of a buoyancy driven fire propagation behind a pyrolysis zone along a vertical wall. *Fire Safety Journal*, 37: 259 – 285.

Wang X, Jiang J, Zhang Y (2007). Numerical study of air movement in a slot-ventilated enclosure. *ASHRAE Transactions*, 113(1): 408 – 413.

Versteeg HK, Malalasekera W (1995). An Introduction to Computational Fluid Dynamics. London: Longman Scientific & Technical.

Yan W, Yang X, Shan M (2009). How to simplify computer simulated persons (CSPs) for modelling personal microenvironments: Comparison and case studies. *ASHRAE Transactions*, 115(1): 473 – 483.

Yang T, Cropper PC, Cook JM, Yousaf R, Fiala D (2007). A new simulation system to predict human-environment thermal interactions in naturally ventilated buildings. Paper presented at the 10th International IBPSA Conference (BS2007), Beijing, China.

Zhai Z, Wang H (2011). Optimizing the trade off between grid resolution and simulation accuracy: Coarse grid CFD modeling. ASHRAE Research project RP – 1418.

Zhai Z, Zhang Z, Zhang W, Chen Q (2007). Evaluation of various turbulence models in predicting airflow and turbulence in enclosed environments by CFD: Part 1: Summary of prevalent turbulence models. *HVAC&R Research*, 13: 853 – 870.

Zukowska D, Popiolek Z, Melikov A (2007). Impact of personal factors and furniture arrangement on the thermal plume above a human body. Paper presented at the 2007 RoomVent Conference, Helsinki, Finland.